Biophysical Journal, Volume *112*

Supplemental Information

Long-Term, Stochastic Editing of Regenerative Anatomy via Targeting Endogenous Bioelectric Gradients

Fallon Durant, Junji Morokuma, Christopher Fields, Katherine Williams, Dany Spencer Adams, and Michael Levin

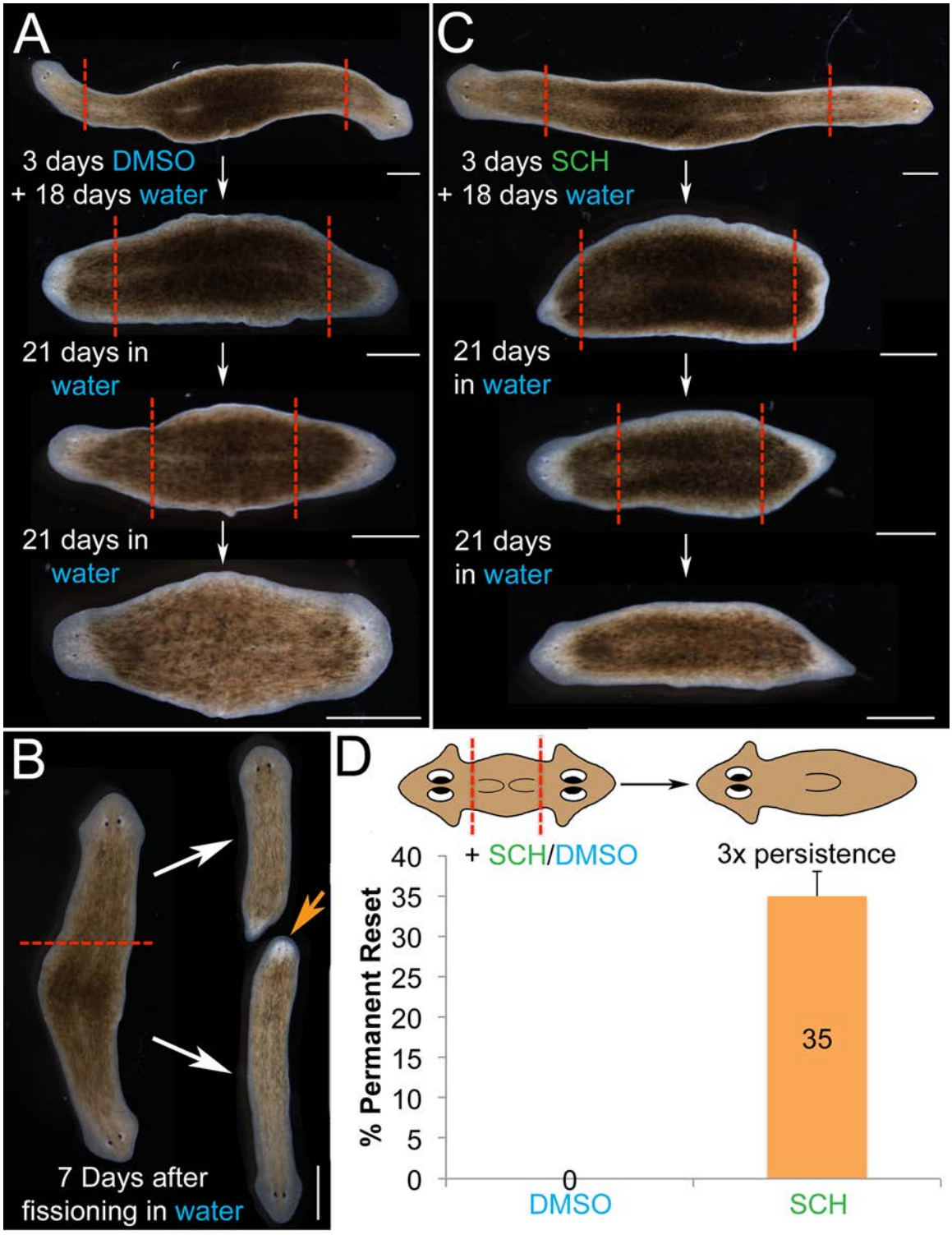

Figure S1: DH phenotype can be reset with bioelectric manipulation.

(A) Planaria that are DH after 8-OH treatment exhibit a permanent change in target morphology. When soaked in only vehicle (DMSO), which does not induce any

patterning defects, recut DH worms regenerate as DH even after three generations of recuts (100%, N=102).

(B) The DH phenotype remains persistent when planaria are allowed to fission on their own, showing that once induced, the phenotype is stable across the most common reproductive mode of this species. Orange arrow indicates second head.

(C) DH, recut, and treated in hyperpolarizing H,K-ATPase inhibitor SCH28080 show a permanent reset of the target morphology back to the SH phenotype (34%, N=102). Similarly, cryptic worms, recut, and treated in SCH28080 show a reduction in the number of DHs regenerated (1%, N=100).

(D) Representation of percent DH that were reset permanently by treatment. Error bars = 95% confidence interval (CIs). Scale bars = 1 mm. SH persisted through three rounds of cutting (34%, N=102), revealing that the change is not to the CRPT (variable) phenotype but to a true, stable WT SH outcome.

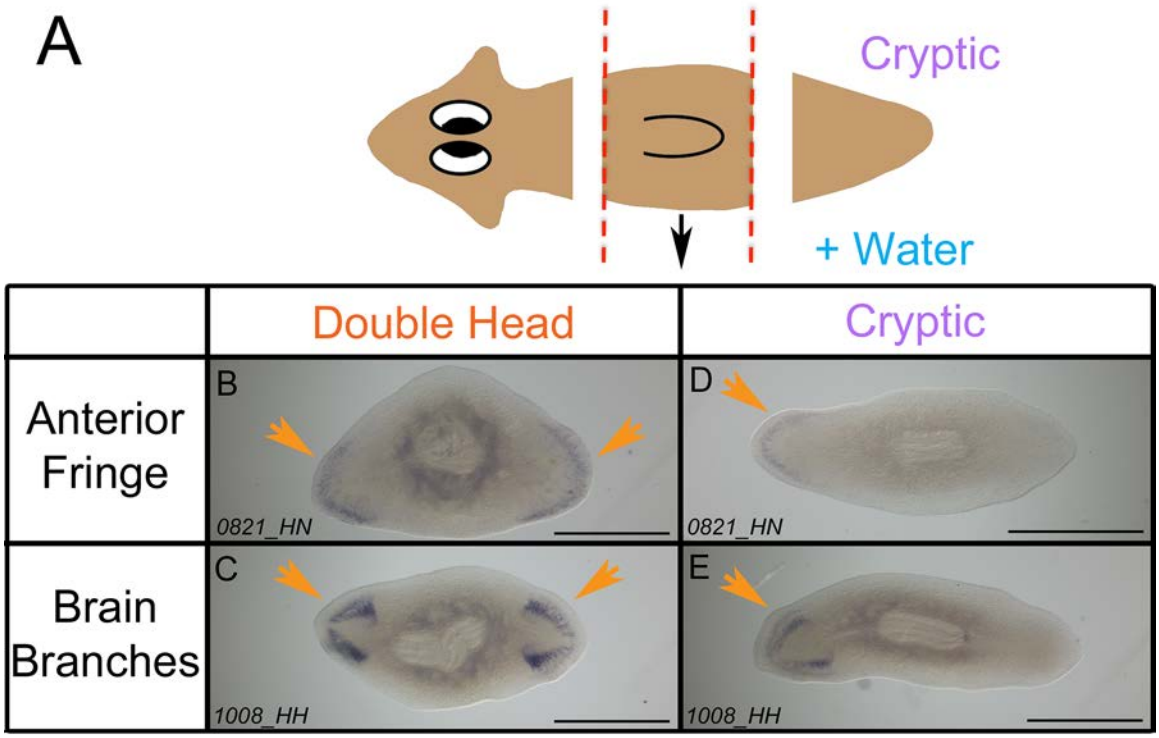

Figure S2: DH worms generated by cutting cryptic worms have true duplicated mature anterior structures.

To confirm that the DH worms indeed have bi-axial anterior structures, tissue specific analyses were performed at 21 days post-amputation (n ≥ 5 for each). (A) Cryptic planaria were cut and allowed to regenerate in water, which produced a population of DH and another population of SH cryptic planaria. (B) The DHs that regenerated from the cryptic planaria exhibit mature chemosensory structures of the anterior fringe (*0821_HN*) (C) as well as mature brain branches (*1008_HH*) on both ends of the planarian (arrowheads), indicating that these planaria are truly DH with complete, mature anterior structures. (D) Resulting SH planaria do not have mature chemosensory structures or (E) mature brain branches in the apparent posterior region of the planarian. Scale bars = 1 mm.

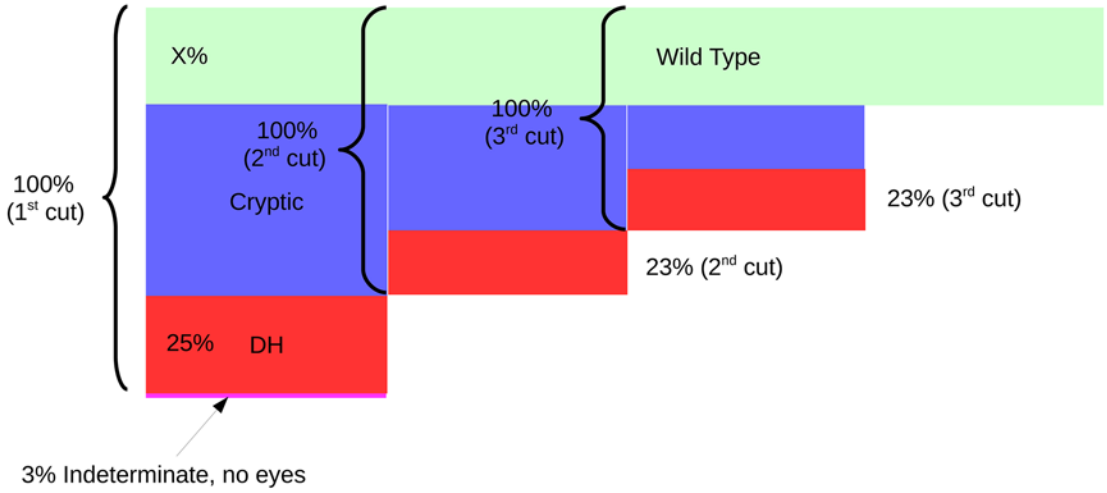

Figure S3: SH regenerates are not WT.

This diagram illustrates in detail why SH regenerates are not WT, by showing the proportion of each type of worm over the first three consecutive cuts. A WT planarian regenerates SH pieces with 100% fidelity. Our experiments show that even normal-looking worms resulting from 8-OH treatment are not truly unaffected, because subsequent cuts result in the same percentage of DH worms, which would never occur if the SH worms were WT. Here we analyze this in more detail, with respect to the dynamics of the three phenotypes in each repeated round of cutting. The null hypothesis is that 8-OH treatment had limited penetrance and SH worms were truly unaffected and remained WT – that a large proportion (X%) of the SH worms will be WT rather than cryptic. This entails that on generation 1 we would have: WT: X%, DH: 25%, Indiscriminate (no eyes): 3%, and Cryptic SH: (72-X)%. Each next round of the experiment is performed on SH worms only, and would contain the assumed X% WT and the (72-X)% cryptics (i.e., 72% of the original population). WT worms do not ever produce DHs when cut in water with no other treatments, so all of the regenerates of WT worms would have to be WT. All the DHs, therefore, must be regenerates of cryptic worms. As this “timecourse” of our experiment illustrates, the fixed WT assumption implies that the fraction of cryptics that regenerate to DH must increase with each generation, even with no additional treatments, which is not observed. Most importantly, after two rounds of amputation in water, our observance of 27% DH from the SH animals is not compatible with the hypothesis that our SH population is WT ($n=30$, $p<0.01$, Fisher’s exact test).

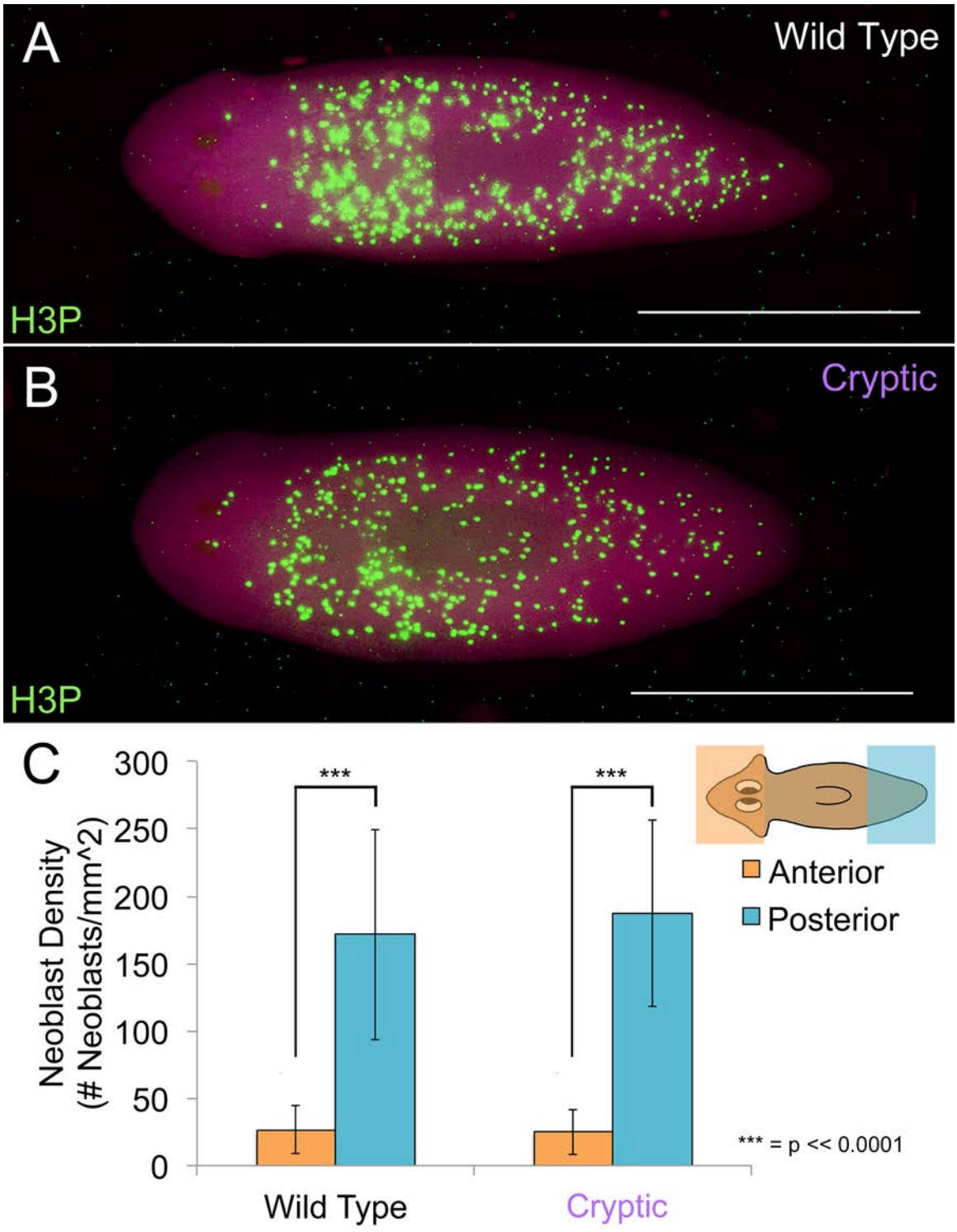

Figure S4: Density of neoblasts in posterior region of cryptic planaria does not resemble anterior neoblast density.

(A-B) WT and cryptic *Dugesia japonica* are devoid of neoblasts (H3P immunohistochemistry) in the region anterior to the eyes. Neoblasts begin immediately posterior to the eyes and extend to the tip of the tail. Neoblasts were counted within a

selection extending to 12% of the total length of the planarian on both anterior and posterior ends using FIJI software ($n \geq 29$) to analyze photos of whole mount transparent worms with all neoblasts and planes visible. Images were threshold adjusted to eliminate background fluorescence. (C) The neoblast density, measured in number of neoblasts/mm^2, was calculated in Excel using FIJI software count and selection area data. Both WT and cryptic planaria showed a significant difference in neoblast density ($p << 0.0001$, two-tailed, unpaired student's t-test) comparing anterior to posterior ends, indicating cryptic tails do not have an anterior-like neoblast distribution. Differences in average neoblast density between WT and cryptic tails are not statistically significant ($p = 0.3369$, two-tailed, unpaired student's t-test) suggesting cryptic tails are more similar to WT tails than heads. Similarly, differences in average neoblast density between WT and cryptic heads are not statistically significant ($p = 0.7813$, two-tailed, unpaired student's t-test). Asterisks = $p << 0.0001$. Error bars = standard deviation. Scale bars = 1 mm.

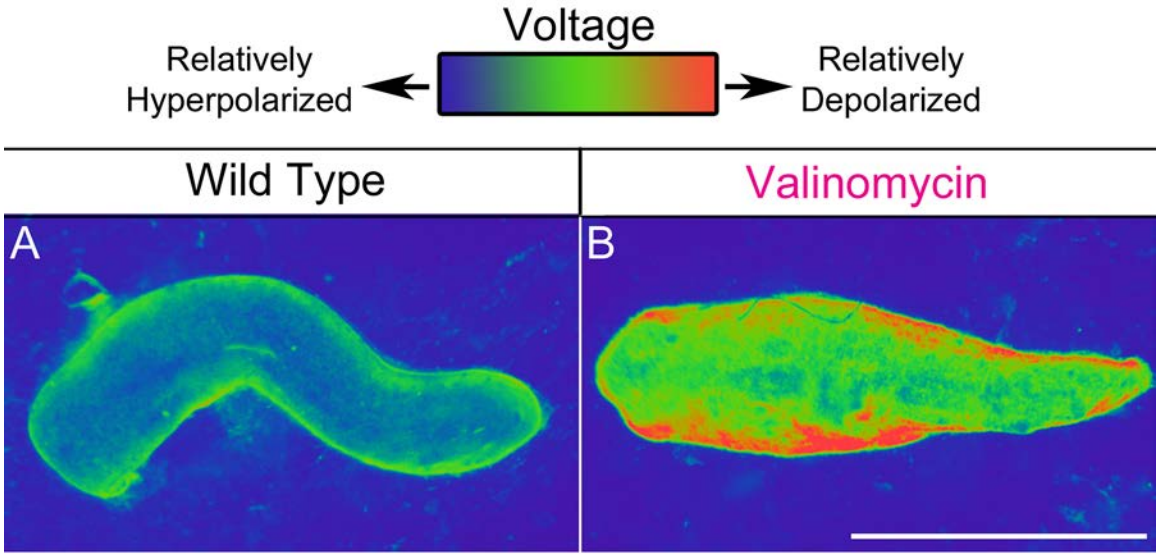

Figure S5: Depolarization via valinomycin + potassium gluconate confirm the ability of DiBAC$_4$(3) to report V$_{mem}$ change

V$_{mem}$ reporter assay using DiBAC$_4$(3) was applied to control vs. depolarizing ionophore-treated worms to confirm that the dye in fact correctly reports V$_{mem}$ change. Images were pseudocolored blue-green-red as with the other dye imaging in this study. Brighter pixels (red) indicate cells that are more relatively depolarized (positively charged) on the inside relative to the outside. Pixels of lower intensity (blue) indicate cells that are more relatively hyperpolarized (negatively charged) on the inside relative to the outside. (A) WT and (B) planaria treated in a 1 µM valinomycin + 150 mM potassium gluconate solution for 1 hour were imaged whole in DiBAC$_4$(3) on a planarian immobilization chip (PIC) (1). Exposure to ionophores depolarizes cells directly, in a much stronger manner than endogenous V$_{mem}$ circuits because they force equalization of positive ions, regardless of the channels or other endogenous bioelectric machinery or cell state. The time course of the experiment had to be very brief because the global depolarization kills the worms rapidly. The DiBAC$_4$(3) fluorescence efficiently reveals the strong depolarizing effects of the ionophore, immediately, even when the worms are not imaged long enough to reveal the endogenous gradients. Upon quantification of intensity values across the whole worm (n = 10 pairs), animals soaked in depolarizing agent were significantly more depolarized than their WT counterparts ($p < 0.05$, unpaired t test), consistent with prior studies using this dye to image voltage (2-11). Scale bars = 1 mm.

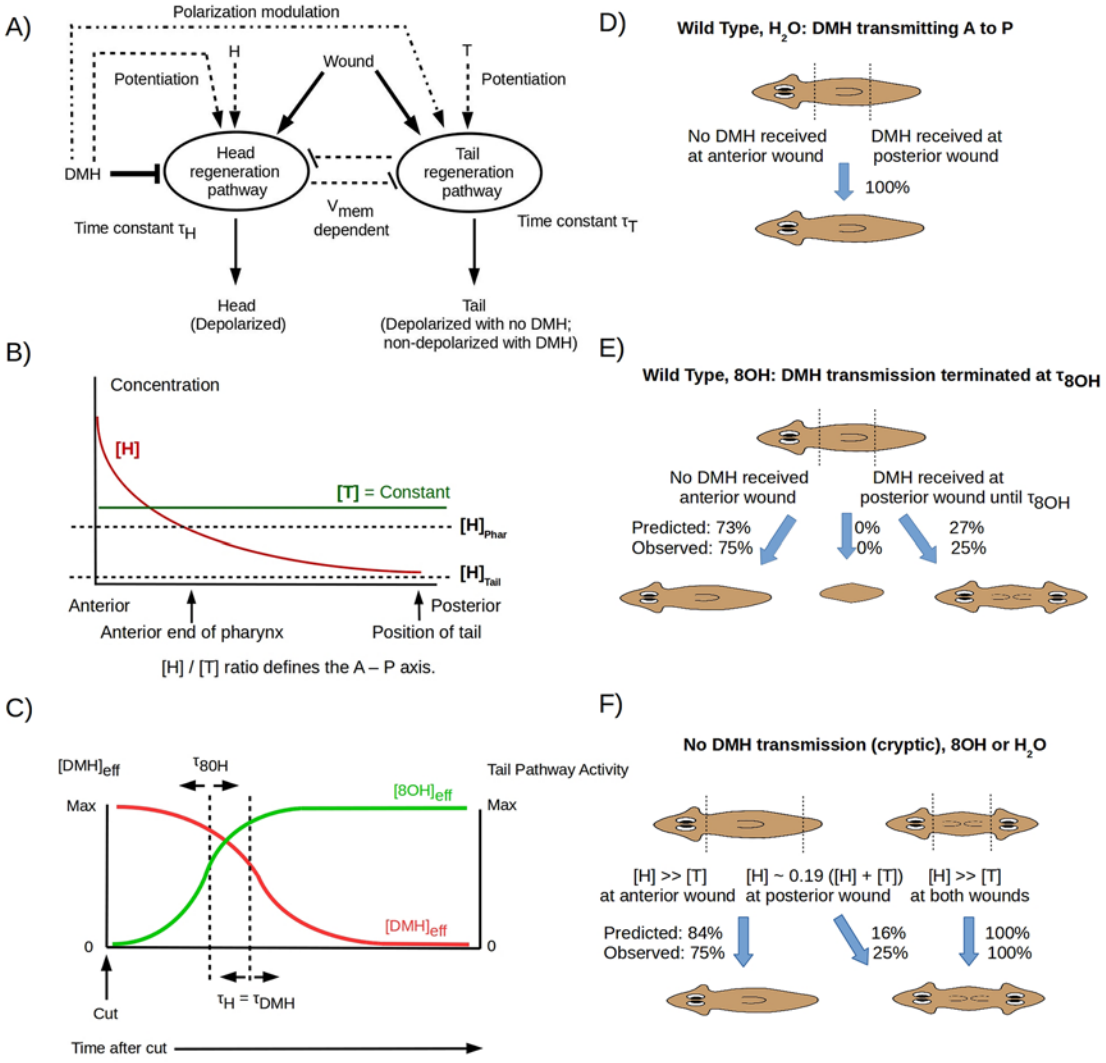

Figure S6: Quantitative model of cryptic–DH branching ratios.

(A) Head and tail regeneration pathways are assumed to be coupled by V_{mem}-dependent mutual inhibition and to both produce depolarized structures by default. Head and tail pathways are quantitatively potentiated by H and T factors, respectively; the head pathway is also potentiated by a "Don't Make Head" (DMH) signal that is actively transmitted in the anterior-to-posterior direction by a V_{mem}- and GJ-dependent mechanism. Wound signal activates potentiated pathways. The DMH signal strongly inhibits the head pathway, and modulates the tail pathway so as to produce a non-depolarized tail. Completed regeneration of head or tail deactivates the head or tail pathway, respectively. The activation time τ_H of the head pathway is shorter than the activation time τ_T of the tail pathway; DMH is assumed to act in a time comparable to τ_H. (B) The ratio of H and T activities, expressible as an effective concentration ratio [H]/[T], decreases along the A/P axis. For simplicity, we assume [H] decreases while [T] remains constant. It is consistent with but not required by the model that [H] = V_{mem}. (C)

The parameter τ_{8OH} / τ_H determines the relation in time between DMH shutoff by 8-OH and inhibition of the head pathway by DMH at the posterior wound. Following DMH shutoff, the head pathway can be activated, producing a DH worm. (D) Simultaneous head and tail amputations of WT animals yield a remnant trunk. No DMH is received at the anterior wound, activating the head pathway. DMH is received at the posterior wound, inhibited the head pathway and allowing the tail pathway to be activated by the wound signal. (E) If head and tail amputation is followed by exposure to 8-OH, the head pathway is initiated normally, in τ_H, at the anterior wound. The head pathway is activated at the posterior wound after τ_{8OH}, i.e. after DMH transmission is shut down, but competes with tail pathway activation during this time. Competition between the pathways produces a stochastic outcome. (F) The morphological outcome of remnant trunk regeneration in cryptic worms with no DMH transmission is determined by the [H]/[T] ratio at the wound sites. See http://chrisfieldsresearch.com/GJ-memory-model.htm for an interactively manipulable version of the model.

Mathematical details of the model

WT worms cut and trunk fragments exposed to 8-OH

At the anterior cut site, anterior-to-posterior DMH transmission is halted immediately. The effective concentration $[DMH]_{eff} = 0$ at the anterior-facing wound of the trunk fragment, allowing the default Head pathway to activate.

At the posterior cut site, anterior-to-posterior DMH transmission continues as long as GJs are operational, inhibiting the Head pathway and allowing Tail pathway activation. Following exposure to 8-OH, DMH transmission stops. The effective transmitted DMH activity thus depends on how soon GJ activity is turned off compared to how fast the Head pathway can activate. Letting τ_{8OH} = time delay from amputation to 8-OH exposure and τ_H = time to activate head pathway, the effective transmitted DMH activity is:

$[DMH]_{sig} = 1/(1 + \exp -10((\tau_{8OH}/\tau_H) – 1.30)))$.

Once DMH transmission is turned off, the residual activity in cells immediately anterior to the posterior wound depends on the posterior cut position x:

$[DMH]_{res} = 1/(1 + \exp 10(x – 0.55))$.

The probability of Head pathway inhibition and hence Tail pathway activation at position x is then:

P_{tail} at $x = [DMH]_{eff}$ at $x = [DMH]_{sig} + [DMH]_{res}$ at x

Normalization gives:

P_{head} at $x = 1 – P_{tail}$ at x

Because $P_{head} = 1$ at the anterior facing wound, the probability of a DH outcome is just P_{head} at the posterior facing wound, i.e. at position x.

Cryptic worms cut and trunk fragments exposed to 8-OH or water

As DMH transmission is off in cryptic worms, the same outcome is expected following exposure to either 8-OH or water. The probability of Head pathway activation then depends only on the ratio of the weak Head (H) and tail (T) factors, which are effectively irrelevant when DMH transmission is active.

For simplicity, we assume that [H] has the same dependence on the posterior cut position as $[DMH]_{res}$ does in a WT animal. In this case, [H] >> [T] at an anterior wound but [H] ~ [T] at a posterior wound. The probability P_{head} at the posterior wound position

x, and hence the probability of a DH outcome, is then just $[DMH]_{res}$ at x scaled by factor representing the relative strengths of the signals:

P_{head} at x = 2.1 $[DMH]_{res}$ at x

Constants in these equations are parameters chosen to fit the x-dependence of the current plus Oviedo *et al.* (2010) data.

Table S1: Cryptic tails are relatively depolarized compared with WT tails

Pair	Wild Type Tail Intensity	Cryptic Tail Intensity	Difference
1	483.8	655.1	171.3
2	396.7	1278.3	881.6
3	619.1	758.4	139.3
4	913.3	1027.2	113.9
5	858.6	1081.3	222.7
6	637.1	1575.8	938.8
7	656.2	2520.1	1863.9
8	762.5	1773.8	1011.3
9	1085.6	1090.7	5.1
10	725.2	752.2	27.0

WT and cryptic planaria were imaged on the same planarian immobilization chip (PIC). Average V_{mem} dye signal intensity was determined via the measure function using FIJI software. A square box proportional to 10% of the total length of the planarian was used to select the most posterior portion of the planarian. Difference between WT and cryptic tail intensity values were calculated using Excel. Each individual cryptic planarian had higher average intensity (relatively depolarized) in the tail region compared to WT and the difference was statistically significant ($p < 0.05$, two-tailed, paired student's t-test). These data represent only those cryptic animals that went on to form DHs. Worms that made SHs upon regeneration were excluded from analysis to enable us to determine what was different about specifically those animals that would change anatomical layout upon cutting.

Supporting References

1. Dexter, J. P., M. B. Tamme, C. H. Lind, and E.-M. S. Collins. 2014. On-chip immobilization of planarians for *in vivo* imaging. *Sci. Rep.* 4.
2. Ozkucur, N., K. P. Quinn, J. C. Pang, C. Du, I. Georgakoudi, E. Miller, M. Levin, and D. L. Kaplan. 2015. Membrane potential depolarization causes alterations in neuron arrangement and connectivity in cocultures. *Brain Behav* 5:24-38.
3. Oviedo, N. J., C. L. Nicolas, D. S. Adams, and M. Levin. 2008. Live Imaging of Planarian Membrane Potential Using $DiBAC_4(3)$. *Cold Spring Harb Protoc* 2008:pdb.prot5055-.
4. Adams, D. S., and M. Levin. 2012. Measuring resting membrane potential using the fluorescent voltage reporters $DiBAC_4(3)$ and CC2-DMPE. *Cold Spring Harbor protocols* 2012:459-464.
5. Adams, D. S., and M. Levin. 2012. General principles for measuring resting membrane potential and ion concentration using fluorescent bioelectricity reporters. *Cold Spring Harbor protocols* 2012:385-397.
6. Epps, D., M. Wolfe, and V. Groppi. 1994. Characterization of the steady-state and dynamic fluorescence properties of the potential-sensitive dye bis-(1,3-dibutylbarbituric acid)trimethine oxonol ($DiBAC_4(3)$) in model systems and cells. *Chem. Phys. Lipids.* 69:137-150.
7. Beane, W. S., J. Morokuma, D. S. Adams, and M. Levin. 2011. A Chemical genetics approach reveals H,K-ATPase-mediated membrane voltage is required for planarian head regeneration. *Chemistry & Biology* 18:77-89.
8. Beane, W. S., J. Morokuma, J. M. Lemire, and M. Levin. 2013. Bioelectric signaling regulates head and organ size during planarian regeneration. *Development* 140:313-322.
9. Adams, D. S., A. Masi, and M. Levin. 2007. H+ pump-dependent changes in membrane voltage are an early mechanism necessary and sufficient to induce Xenopus tail regeneration. *Development* 134:1323-1335.
10. Levin, M., T. Thorlin, K. R. Robinson, T. Nogi, and M. Mercola. 2002. Asymmetries in H+/K+-ATPase and cell membrane potentials comprise a very early step in left-right patterning. *Cell* 111:77-89.
11. Vandenberg, L. N., R. D. Morrie, and D. S. Adams. 2011. V-ATPase-dependent ectodermal voltage and pH regionalization are required for craniofacial morphogenesis. *Dev Dyn* 240:1889-1904.